Article

Journal of
Nanoscience and Nanotechnology
Vol. 16, 9085–9092, 2016
www.aspbs.com/jnn

Tunable Mesoporous Phenolic-Silica Composites Templated by Poly(ethylene oxide-*b*-ε-caprolactone) Block Copolymer

Wei-Cheng Chu[1], Lizong Dai[2], Jem-Kun Chen[3], Chih-Feng Huang[4], and Shiao-Wei Kuo[1, 5, *]

[1] *Department of Materials and Optoelectronic Science, Center for Nanoscience and Nanotechnology, National Sun Yat-Sen University, Kaohsiung, 804, Taiwan*
[2] *Fujian Provincial Key Laboratory of Fire Retardant Materials, College of Materials, Xiamen University, Xiamen, 361005, China*
[3] *Department of Materials Science and Engineering, National Taiwan University of Science and Technology, Taipei, 106, Taiwan*
[4] *Department of Chemical Engineering, National Chung Hsing University, Taichung, 402, Taiwan*
[5] *School of Chemical Engineering, East China University of Science and Technology, Shanghai, 200237, China*

In this study, we prepared mesoporous composite materials templated by poly(ethylene oxide-*b*-ε-caprolactone) (PEO-*b*-PCL) diblock copolymers with the matrix of TEOS and phenolic resin. Clearly, the TEOS is inorganic source and the phenolic resin is organic source, hydrogen-bond donor, and expander. The phenolic resin exists in a matrix of the silica wall or hole of silica matrix. Through the DSC thermograms, the morphology of composite nanostructure can be forecasted by supercooling temperature. Small-angle X-ray scattering, transmission electron microscopy, and N_2 sorption measurements indicates that the mesoporous composites displayed the morphology of short cylindrical mesostructure. The morphology of mesoporous composite materials is greatly affected by the phenolic resins that are the large pore size (ca. 30∼40 nm) short cylinder structure, indicates its possibility of potential application separation, low-refractive index and low-dielectric materials.

Keywords: Mesoporous Composite, PEO-*b*-PCL, EISA, Phenolic Resin.

1. INTRODUCTION

Mesoporous materials have received great attention due to their unique properties including high surface area, large pore volume, mechanical stability and various applications in adsorption, catalysis, drug delivery and separation.[1–4] Initially, (Mobil Composition of Matter No. 41) MCM-41s and (Santa Barbara Amorphous No. n) SBA-n series were fabricated using aqueous solutions; however, limiting the templated surfactants that could dissolve in aqueous solutions.[5–8] However, the most amphiphilic diblock copolymers are water-insoluble, and the evaporation-induced self-assembly strategy becomes important to broadly use for the preparation of mesoporous materials. Poly(ethylene oxide)-*b*-poly(propylene oxide)-*b*-poly(ethylene oxide) triblock copolymers as templates have been widely preparing many highly ordered large-pore mesoporous materials.[9–12] Zhao et al. used poly(ethylene oxide-*b*-styrene) (PEO-*b*-PS) block copolymer to prepare the highly order mesoporous silica materials.[13] In our previous studies, we used a series of amphiphilic block copolymers including poly(ethylene oxide-*b*-ε-caprolactone) (PEO-*b*-PCL), poly(ethylene oxide-*b*-Lactide) (PEO-*b*-PLA) and poly(ethylene-*b*-ethylene oxide-*b*-ε-caprolactone) (PE-*b*-PEO-*b*-PCL) with different molecular weights as the templates to prepare ordered mesoporous materials.[14–19]

In addition, the amphiphilic block copolymers are broadly used in thermosets have been prepared mesoporous organic or carbon materials.[20–25] Reaction-induced microphase separation strategy is broadly used for the preparation of mesoporous phenolic resin and carbon materials.[26–29] Hu et al. reported the nanostructures formation in phenolic from the Novolac type of phenolic

*Author to whom correspondence should be addressed.

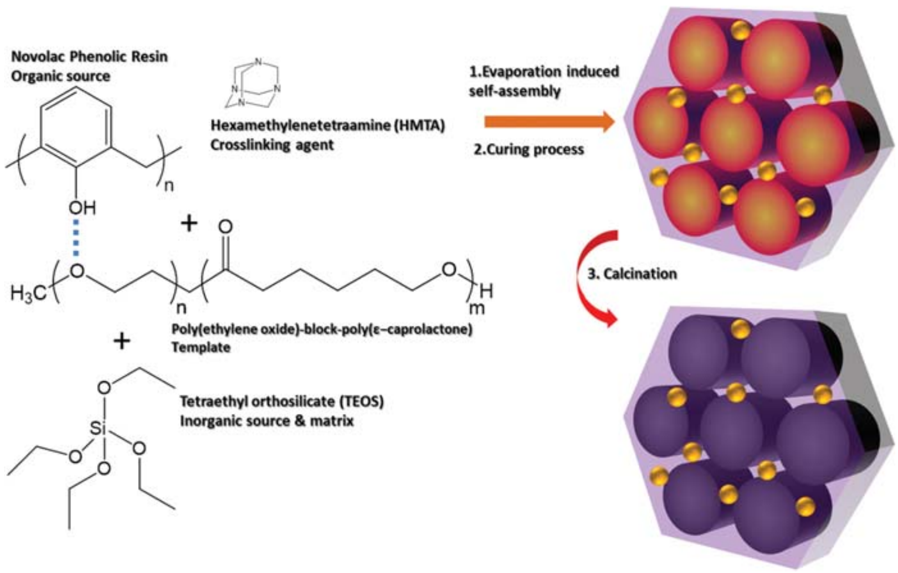

Scheme 1. Preparation of mesoporous composite materials.

resin and PEO-*b*-PS diblock copolymer, cured with HMTA. The use of a Novolac type of phenolic resin can allow studying the morphological transitions before and after curing reaction.[30] In our previous studies, we have also investigated the molecular weight effect templated by PEO-*b*-PCL on the fabrication of ordered mesoporous phenolic resins and polybenzoxazines through the reaction-induced microphase separation strategy.[20–29] The composite materials of organic (polymer)–inorganic (silica) is very important, since the semiconductor package parts such as printed circuit boards and resin adhesive, consist of organic–inorganic (polymer-silica) hybrid materials. Such materials provide favorable low-dielectric properties as reflected and low-refractive index by porous properties. Applying mesoporous silica material to exploit its porous properties can be accomplished in two ways: first way is used, chemical or vapor deposition, and second way is using composites with polymers.[31–44] As a result, the mesoporous composite materials can improve this application. In this study (Scheme 1), we use the second way by blending with the phenolic resin, HMTA, PEO-*b*-PCL and TEOS to prepare the mesoporous composite materials. The pore sizes of mesoporous composite materials were larger than mesoporous silica materials only templated by PEO-*b*-PCL. The phenolic resin has hydrogen bonding interaction with PEO segment and PEO is hydrophilic segment during mechanical composite processing. The hydrogen bonding of phenolic and templates induce the pore size increased and the phase transition.[24] Finally, the phenolic resin exists in a matrix of the silica wall or hole of mesoporous silica. This material has potential applications including separation, low-dielectric and low-refractive index.

2. EXPERIMENTAL SECTION

2.1. Materials

Monomethoxy-poly(ethylene glycol) (PEO, $M_w = 5,000$) was obtained from Aldrich. The ε-Caprolactone (ε-CL, 99%, Aldrich) was purified by vacuum distillation with CaH_2 at ca. 97 °C and 5 mm-Hg. Stannous(II) octoate ($Sn(Oct)_2$, 100%, Alfa Aesar) was used as catalyst. Phenolic resin was synthesized with sulfuric acid catalyst by a condensation reaction where average molecular weight was 500. Dichloromethane (DCM), n-hexane, tetrahydrofuran (THF), tetraethyl orthosilicate (TEOS), hydrochloric acid (HCl) and hexamethylenetetramine (HMTA) were all from Aldrich.

2.2. Synthesis of PEO-*b*-PCL Block Copolymer

Diblock copolymers was prepared with the monomer of ε-CL, the macro-initiator of monomethoxy-poly(ethylene glycol) and $Sn(Oct)_2$ as the catalyst through the ring-opening polymerization in toluene under an N_2 atmosphere at 140 °C. After 18 hours, the resulting block copolymer was dissolved in dichloromethane and then precipitated in an excess of cold n-hexane 3 times circle. The polymers were dried at 40 °C under vacuum. Yield: 85%; ^{1}H NMR (500 MHz, $CDCl_3$,): δ 4.10 (t, OCH_2, PCL), 3.65 (s, CH_2CH_2O, PEO), 3.35 (s, OCH_3, PEO), 2.30 (t, 2H, PCL), 1.63 (m, 4H, PCL), 1.38 (m, 2H, PCL). The molecular weight was determined by GPC (PDI = 1.19, $M_w = 32,000$) and ^{1}H NMR ($M_w = 14,900$, $EO_{114}CL_{87}$).

2.3. Synthesis of Mesoporous Composite

The blending compositions used in this study are summarized in Table I. THF was slowly evaporated at room temperature, and the samples were subsequently in vacuum

Table I. Blending composition of mesoporous composites.

Sample	TEOS (g)	PEO-*b*-PCL (g)	Phenolic resin (mg)	HMTA (mg)	THF (g)	0.1 M $HCl_{(aq)}$ (g)
TEP1	0.07	0.1	10	1	5	0.1
TEP2	0.07	0.1	7.5	0.7	5	0.1
TEP3	0.07	0.1	5	0.5	5	0.1
TEP4	0.09	0.1	10	1	5	0.1
TEP5	0.09	0.1	7.5	0.7	5	0.1
TEP6	0.09	0.1	5	0.5	5	0.1
TEP7	0.11	0.1	10	1	5	0.1
TEP8	0.11	0.1	7.5	0.7	5	0.1
TEP9	0.11	0.1	5	0.5	5	0.1
TEP10	0.11	0.1	–	–	5	0.1

dried at 30 °C for one day. Phenolic resin, HMTA, PEO-*b*-PCL and TEOS as the silica precursor were dissolved in THF until the solutions were homogenous. Mesoporous silica materials were prepared through an EISA strategy in THF, using PEO-*b*-PCL copolymers as templates and TEOS. Phenolic resin, HMTA and TEOS were added into a THF (5 g) solution of the block copolymer (2.0 wt%, containing 0.10 g of copolymer). Various TEOS–to–PEO-*b*-PCL was used at a constant 0.1 g of 0.1 M $HCl_{(aq)}$ concentration into the homogenous solution, with stirring, which was continued for 30 min. The sample was poured into an aluminum dish and the THF was evaporated at room temperature for 48 hours. The transparent film was collected and ground into a powder, which was then transferred to a PFA bottle containing 1.0 M $HCl_{(aq)}$ (30 mL) and treated hydrothermally at 100 °C for 48 hours. The product was washed with Di-water and EtOH, dried at room temperature, and curing of the samples was performed using the following temperature profile (100 °C for 2 hours, 150 °C for 2 hours, and 190 °C for 0.5 hours). Pyrolysis of the crosslinked samples without a protective gas atmosphere was performed by slowly heating from room temperature to 330 °C at a heating rate of 1 °C/min.

2.4. Characterization

The molecular weights was determined by the gel permeation chromatography (GPC) using a Waters 510 high-performance liquid chromatograph equipped with a 410 differential refractometer and three Ultrastyragel columns connected in series, with DMF as the eluent (flow rate: 0.5 mL/min). ^{1}H NMR spectra were measured using a Varian UNITY INOVA-500 (500 MHz) spectrometer, with the residual proton resonance of the deuterated chloroform solvent acting as the internal standard. Small-angle X-ray scattering (Bruker AXS, Karlsruhe, Germany) with Cu Kα radiation (30 W, 50 kV, 600 μA) was used to measure the d-spacing. Transmission electron microscope (TEM, JEOL 3010, operated at 200 kV) was used to observe the morphology of mesoporous silicas and TEM samples for measurement were suspended in ethanol and supported onto a holey carbon film Cu grid. Nitrogen adsorption–desorption isotherms were measured using an ASAP 2020 analyzer. The Barrett–Joyner–Halenda (BJH) model was used to calculate pore volumes, pore size distributions and the specific surface areas.

3. RESULTS AND DISCUSSION

3.1. Characterization of Composite

Differential scanning calorimetry (DSC) is a convenient to determine the miscibility of composite including the block copolymer, phenolic resin and silica matrix before the calcination. Table II summarizes the thermal properties of composite based on DSC analyses. Figure 1 shows the second-runs heating (heating rate: 20 °C/min) in the DSC thermograms, and the values of glass transition temperature (T_g) of the PEO and PCL are very similar c.a. −60 °C, so the miscibility between PEO and PCL cannot be determined from the number of glass transitions. The melting temperatures become broad being caused by morphological effects and hydrogen bonding interaction with phenolic resins. The two T_gs of PEO and PCL segments were found that the higher and lower T_g are coming from the phenolic-PEO and the phenolic-PCL phases because the inter-association equilibrium constant (K_A)

Table II. Thermal properties of mesoporous composites.

Sample	T_g (°C)		T_m (°C)
PEO-*b*-PCL	−60		52.2
TEP1	−45.5	−13.0	50.1
TEP2	−44.0	9.2	49.2
TEP3	−44.0	–	47.8
TEP4	−51.7	12.0	50.6
TEP5	−51.7	13.3	49.6
TEP6	53.6	26.0	50.1
TEP7	−43.0	4.7	51.5
TEP8	−45.9	10.0	50.6
TEP9	−51.6	–	49.6

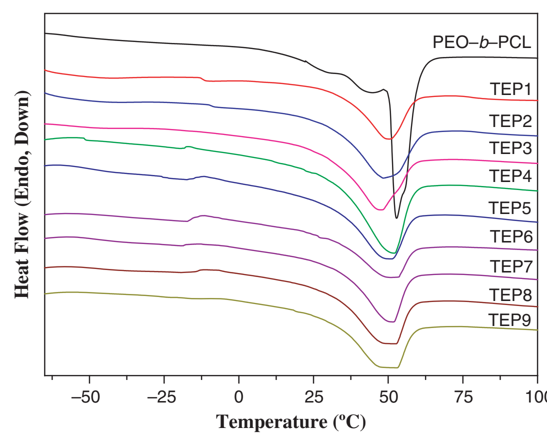

Figure 1. DSC heating curves of mesoporous composites templated by PEO-*b*-PCL at different weight fractions of TEOS/PEO-*b*-PCL/phenolic after curing HMTA.

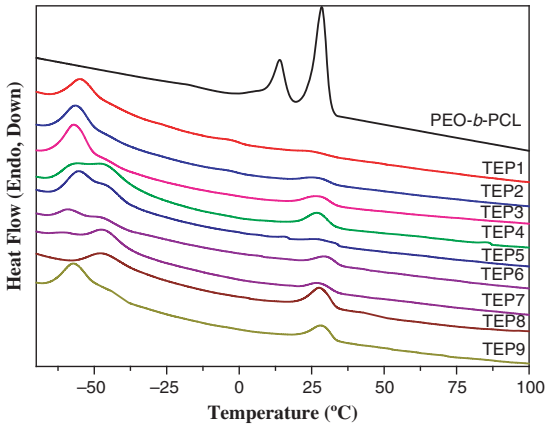

Figure 2. DSC cooling curves of mesoporous composites templated by PEO-*b*-PCL at different weight fractions of TEOS/PEO-*b*-PCL/phenolic after curing HMTA for with a constant cooling rate of 5 °C/min.

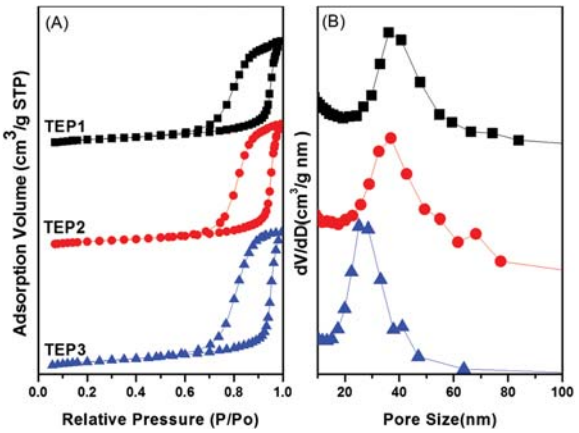

Figure 4. (a) N_2 adsorption/desorption isotherms and (b) pore size distribution curves of mesoporous composites TEP1, TEP2 and TEP3 templated by PEO-*b*-PCL.

between phenolic hydroxyl group and PEO ether group is greater than the inter-association equilibrium constant between PCL carbonyl group. Clearly, the T_g of PCL segment shifts increasing higher value with the increase of phenolic contents, but the T_g of PEO segment did not trend with the increase of phenolic contents since the T_g of PEO segment also depends on the crystalline of PEO block segment.

Figure 2 shows the first-runs cooling (cooling rate: 5 °C/min) in the DSC thermograms, and the freezing temperature (T_f) defines the peak of the crystallization exotherm. The higher and lower crystallization peaks T_f of the pure PEO-*b*-PCL with are corresponding to PEO segment and PCL segment, respectively. Previous reports proofed the T_f with the nonisothermal crystallization under

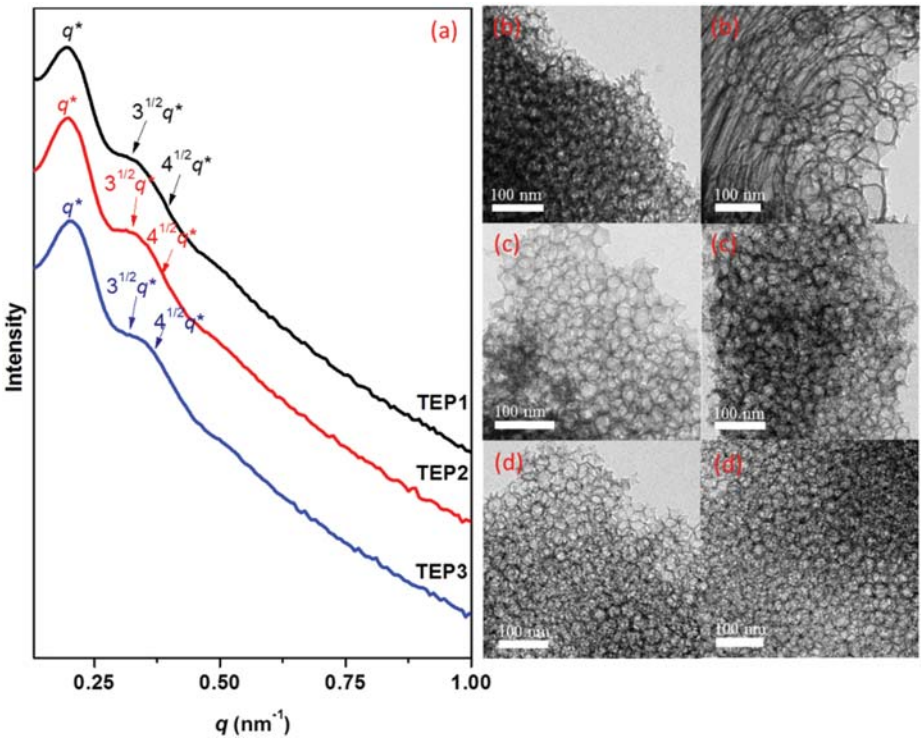

Figure 3. (a) SAXS patterns and (b–d) TEM images of mesoporous composites templated by PEO-*b*-PCL at weight fractions of (b) TEP1, (c) TEP2, (d) TEP3.

Table III. Textural properties of mesoporous composites templated by various block copolymers.

Sample	d (nm)[a]	Pore size (nm)	S_{BET} (m^2/g)[b]	S_M (m^2/g)[b]	Pore volume (cm^3/g)	Micropore volume (cm^3/g)	Morphology
TEP1	33.1	37.4	311.3	36.5	1.20	0.014	Short cylinder
TEP2	32.4	36.8	331.9	39.1	1.18	0.014	Short cylinder
TEP3	31.8	26.1	318.5	41.6	1.11	0.016	Short cylinder
TEP4	37.6	32.8	362.3	27.2	1.55	0.009	Short cylinder
TEP5	31.3	32.3	379.4	43.3	1.50	0.017	Short cylinder
TEP6	30.8	29.3	333.0	59.3	1.11	0.025	Short cylinder
TEP7	28.5	33.7	301.3	34.4	1.39	0.013	Short cylinder
TEP8	28.5	32.2	280.2	28.9	1.21	0.011	Short cylinder
TEP9	28.5	28.7	400.7	40.4	1.39	0.015	Short cylinder
TEP10	25.1	17.9	575.8	94.1	0.65	0.082	Long cylinder

Notes: [a]The d-spacing values were calculated from the first SAXS peak by the formula $d = 2\pi/q^*$. [b]S_{BET} and S_M are the total BET surface area and micropore surface area calculated from the t-plots, respectively.

a fixed cooling rate and displays a different correlation with the microdomain structure.[45–50] It has reported that the degree of supercooling ($\Delta T = T_m^0 - T_f$) required to initiate crystallization in the lamellar microdomains ($\Delta T =$ 50 °C) as a 1D lamellar confinement and exceedingly large undercoolings is required for crystallizations in the cylindrical microdomains ($\Delta T = 125$ °C) a 2D cylindrical confinement.[45–50] In order words, the exotherm at a lower T_f (c.a. $-55 \sim -45$ °C) is the PCL segment in a 2D cylindrical confinement. The DSC analyses are able to become more convenient characterize the morphology of composite nanostructure between crystalline–crystalline diblock copolymer and organic–inorganic matrix, but the way cannot use in a diblock copolymer of amorphous hydrophobic segment.

3.2. Characterization of Mesoporous Composite

To study the hydrogen bonding effect of the phenolic resin in diblock copolymers PEO-*b*-PCL during the EISA process used for the synthesis of mesoporous composite, we prepared different composition featuring different phenolic resin and TEOS (Table I). Figure 3 displays SAXS patterns of the mesoporous composite templated by $EO_{114}CL_{87}$ at various $EO_{114}CL_{87}$–to–phenolic resin weight ratios at fixed

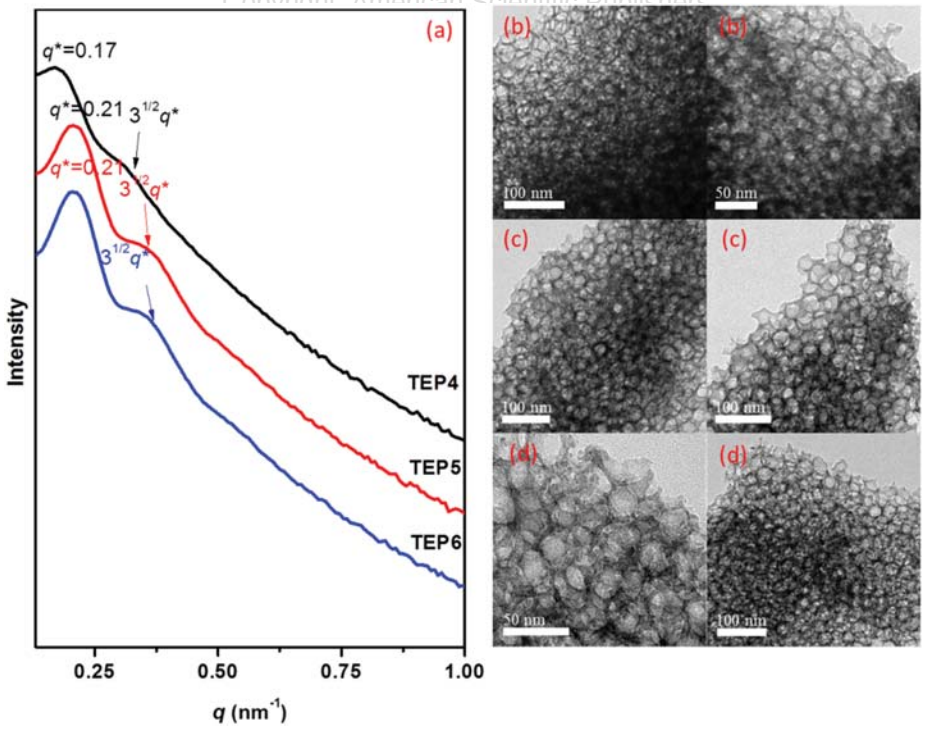

Figure 5. (a) SAXS patterns and (b–d) TEM images of mesoporous composites templated by PEO-*b*-PCL at weight fractions of (b) TEP4, (c) TEP5, (d) TEP6.

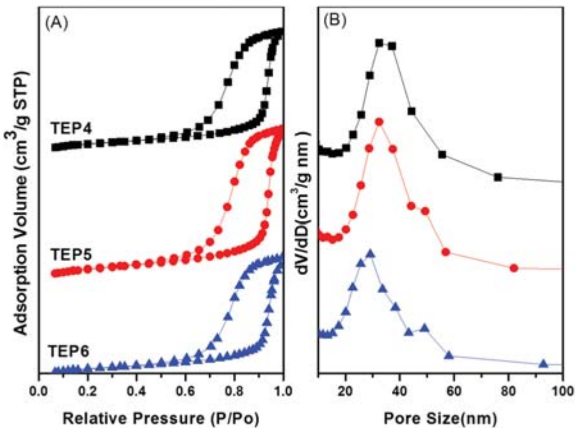

Figure 6. (a) N_2 adsorption/desorption isotherms and (b) pore size distribution curves of mesoporous composites TEP4, TEP5 and TEP6 templated by PEO-*b*-PCL.

TEOS; the primary scattering peaks appeared clear values of q of q^*, $3^{1/2}q^*$ and $4^{1/2}q^*$ for all composition, suggesting morphologies: short-cylinder structures. In agreement, the TEM images in Figures 1(b–d) reveal short-cylinder mesoporous materials, with the distance between each lamellar silica wall being much larger than the short cylindrical mesopores. Increasing the ratio of phenolic resin from TEP3 sample to sample TEP1, the pore being swelled was evident in the TEM images in Figures 1(b–d).

The N_2 adsorption and desorption isotherms of mesoporous composite materials all featured representative type-IV curves according the BDDT (Brunauer, Deming, Deming, and Teller) system, with a capillary condensation steps (Fig. 4(a)), and composition provided a capillary condensation step in the relative pressure range from 0.6 to 1.0, accordingly displaying a typical H_3-like hysteresis loop, characteristic of slit-like mesostructure, indicating a sharp pore size distribution at ca. 19 nm based on the Harkins and Jura model, showed in Figure 4(b). Table III summarizes the d-spacing, Barrett-Joyner-Halenda (BJH) pore size distributions; BET surface areas, mircopore surface area, pore volumes, and mircopore pore volumes of the materials. Increasing the ratio of phenolic resin from TEP3 sample to sample TEP1, the pore sizes were increased showed in Table III.

Figure 5 display the TEM images and SAXS patterns of the mesoporous composite materials. The SAXS pattern in Figure 5(a) for TEP4 features its maximum intensity at a value of q^* of approximately 0.17 nm^{-1} (d = 37.6 nm) and the scattering peaks appeared clear values of q of q^*, $3^{1/2}q^*$ and $4^{1/2}q^*$; a short-cylinder structure appears in the corresponding TEM image (Fig. 5(b)). Further decreasing the phenolic resin weight ratio caused the primary SAXS peak to gradually shift to higher values of q^* and become sharper, indicating that the d-spacing gradually change to 30.8 nm and that the mesoporous silica became more ordered. These features were also evident in

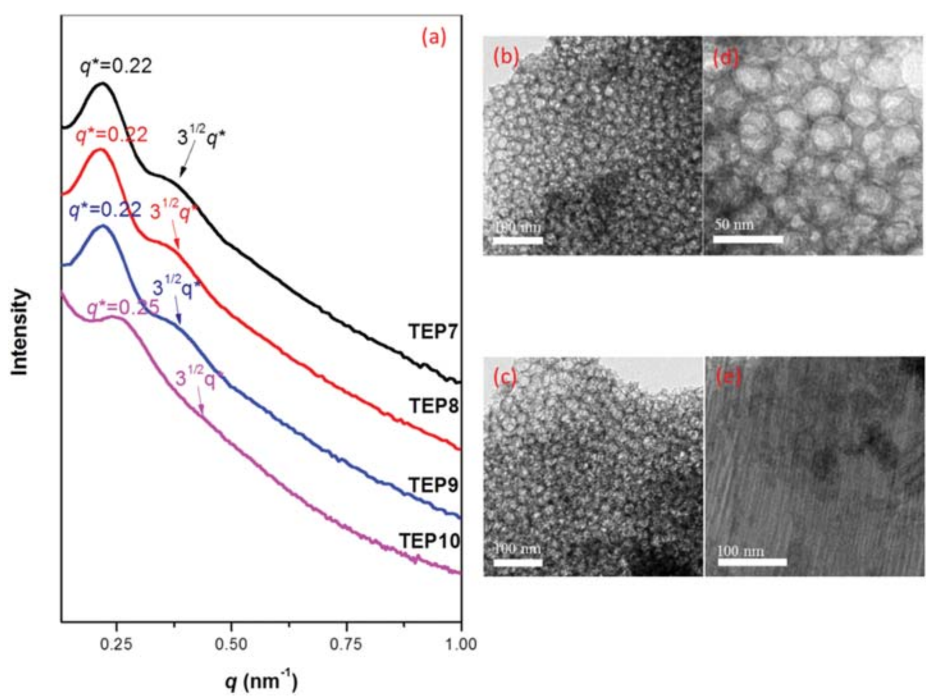

Figure 7. (a) SAXS patterns and (b–d) TEM images of mesoporous composites templated by PEO-*b*-PCL at weight fractions of (b) TEP7, (c) TEP8, (d) TEP9, (d) TEP10.

the TEM images in Figures 5(b–d), with the mesoporous structures becoming order decreasing the phenolic resin content.

In Figure 6(a), the mesoporous composite materials (TEP4–TEP6) prepared at the different phenolic resin weight ratios all provided typical type-IV in their N_2 adsorption and desorption isotherms curves according the BDDT system. They all exhibited H_3-like hysteresis loops at values of P/P_0 ranging from 0.5 to 1.0, indicative of typical mesoporous structures with slit-like pores (short-cylinder structure). Figure 6(b) displays the pore size distributions measured from the adsorption curves, based on the Harkins and Jura model. For TEP4, TEP5 and TEP6, the pore size distributions were 32.8, 32.3 and 29.3 nm, respectively. Decreasing the ratio of phenolic resin from TEP4 sample to sample TEP6, the pore sizes were decreased showed in Figure 6(b).

Figure 7 displays the SAXS patterns and TEM images of mesoporous composites obtained from the systems templated by di-block copolymer PEO-*b*-PCL at various TEOS/template = 1.1/1 weight ratios with different phenolic resin. The mesoporous silica of TEP10 does not have phenolic resin. The *d*-spacing of TEP10 was an identical 25.1 nm ($q^* = 0.25$ nm^{-1}) and the others were an identical 28.5 nm ($q^* = 0.22$ nm^{-1}). Clearly, the mesoporous composite materials of TEP6, TEP7 and TEP9 behaved the short cylinder mesostructure at all ratios and both of SAXS pattern (in Fig. 7(a)) and TEM image (Figs. 7(b–d)) are agreeable. But the mesoporous silica material of TEP10 behaved the long cylinder mesostructure in TEM imager (Figs. 7(e)).

N_2 adsorption and desorption isotherms curves as shown in Figure 8(a) of mesoporous composite exhibits typical type-IV curves according the BDDT system with an H_3-type hysteresis loop, suggesting a slit-like mesostructure. A sharp capillary condensation in the relative pressure between 0.5 and 1.0 is observed, indicating TEP7, TEP8 and TEP9 pore size distribution centered at 33.7, 32.2 and 28.7 nm, respectively (Fig. 8(b)). In addition, a sharp capillary condensation in the relative pressure between 0.4 and 1.0 is observed, indicating TEP10 pore size distribution centered at 17.9 nm. Decreasing the ratio of phenolic resin from TEP7 sample to sample TEP10, the pore sizes were decreased.

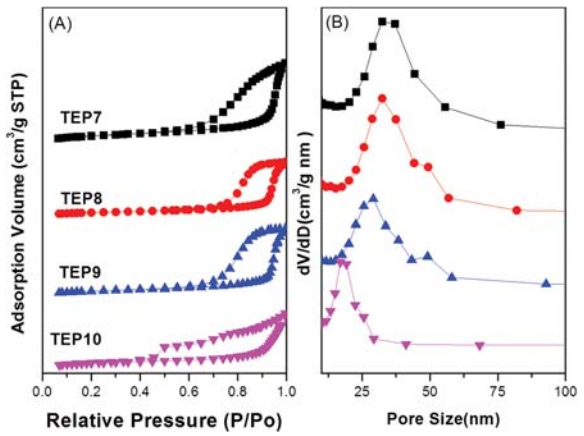

Figure 8. (a) N_2 adsorption/desorption isotherms and (b) pore size distribution curves of mesoporous composites TEP7, TEP8 and TEP9 templated by PEO-*b*-PCL.

4. CONCLUSIONS

Mesoporous organic–inorganic composite materials are synthesized by one-step blended with the PEO-*b*-PCL, TEOS, phenolic resin, HMTA. During the EISA strategy, the phenolic resin plays an expanded role because the hydroxyl group of phenolic resin and an ether group of PEO segments possesses the hydrogen bonding to make the pore size swelled and the phase transition from long cylinder mesostructure to short cylinder mesostructure. After the curing and the calcination, the phenolic resin exists in a matrix of the silica wall or hole of silica matrix. Through the DSC cooling results, the morphology of composite nanostructure can be forecasted by supercooling temperature. The SAXS patterns, TEM image and nitrogen isotherm curve show that all of the mesoporous composite materials are the large pore size (c.a. 30∼40 nm) with short cylinder structure, indicating its possibility of potential application separation, low-refractive index and low-dielectric materials.

Acknowledgment: This work was supported financially by the Ministry of Science and Technology, Taiwan, Republic of China, under Contract No. MOST 103-2221-E-110-079-MY3 and was also supported by the National Natural Science Foundation of China (U1205113), Scientific and Technological Innovation Platform of Fujian Province of China (2014H2006).

References and Notes

1. D. Arcos, A. Lopez-Noriega, E. Ruiz-Hernandez, O. Terasaki, and M. Vallet-Regi, *Chem. Mater.* 21, 1000 (**2009**).
2. A. P. Katsoulidis and M. G. Kanatzidis, *Chem. Mater.* 24, 471 (**2012**).
3. A. Popa, V. Sasca, and I. Holclajtner-Antunovic, *Microporous Mesoporous Mater.* 156, 127 (**2012**).
4. H. J. Wang, L. Wang, T. Sato, Y. Sakamoto, S. Tominaka, K. Miyasaka, N. Miyamoto, Y. Nemoto, O. Terasaki, and Y. Yamauchi, *Chem. Mater.* 24, 1591 (**2012**).
5. J. S. Beck, J. C. Vartuli, W. J. Roth, M. E. Leonowicz, C. T. Kresge, K. D. Schmitt, C. T. W. Chu, D. H. Olson, E. W. Sheppard, S. B. McCullen, J. B. Higgins, and J. L. Schlenker, *J. Am. Chem. Soc.* 114, 10834 (**1992**).
6. C. T. Kresge, M. E. Leonowicz, W. J. Roth, J. C. Vartuli, and J. S. Beck, *Nature* 359, 710 (**1992**).
7. D. Y. Zhao, J. L. Feng, Q. S. Huo, N. Melosh, G. H. Fredrickson, B. F. Chmelka, and G. D. Stucky, *Science* 279, 548 (**1998**).
8. D. Y. Zhao, Q. S. Huo, J. L. Feng, B. F. Chmelka, and G. D. Stucky, *J. Am. Chem. Soc.* 120, 6024 (**1998**).

9. V. Malgras, Q. Ji, Y. Kamachi, T. Mori, F. K. Shieh, K. C. W. Wu, K. Ariga, and Y. Yamauchi, *Bull. Chem. Soc. Jpn.* 88, 1171 (**2015**).
10. K. Kailasam, Y. S. Jun, P. Katekomol, J. D. Epping, W. H. Hongand, and A. Thomas, *Chem. Mater.* 22, 428 (**2010**).
11. R. L. Liu, Y. F. Shi, Y. Wan, Y. Meng, F. Q. Zhang, D. Gu, Z. X. Chen, B. Tu, and D. Y. Zhao, *J. Am. Chem. Soc.* 128, 11652 (**2006**).
12. C. Urata, Y. Tamura, Y. Yamauchi, and K. Kuroda, *J. Mater. Chem.* 21, 3711 (**2011**).
13. Y. H. Deng, T. Yu, Y. Wan, Y. F. Shi, Y. Meng, D. Gu, L. J. Zhang, Y. Huang, C. Liu, X. J. Wu and D. Y. Zhao, *J. Am. Chem. Soc.* 129, 1690 (**2007**).
14. J. G. Li and S. W. Kuo, *RSC Adv.* 1, 1822 (**2011**).
15. J. G. Li, Y. H. Chang, Y. S. Lin, and S. W. Kuo, *RSC Adv.* 2, 12973 (**2012**).
16. J. G. Li, W. C. Chu, C. W. Tu, and S. W. Kuo, *J. Nanosci. Nanotechnol.* 13, 2495 (**2013**).
17. W. C. Chu, S. F. Chiang, J. G. Li, and S. W. Kuo, *RSC Adv.* 4, 784 (**2014**).
18. C. C. Liu, J. G. Li, and S. W. Kuo, *RSC Adv.* 4, 20262 (**2014**).
19. O. Altukhov and S. W. Kuo, *RSC Adv.* 5, 22625 (**2015**).
20. M. A. Hillmyer, P. M. Lipic, D. A. Hajduk, K. Almdal, and F. S. Bates, *J. Am. Chem. Soc.* 119, 2749 (**1997**).
21. P. M. Lipic, F. S. Bates, and M. A. Hillmyer, *J. Am. Chem. Soc.* 120, 8963 (**1998**).
22. J. G. Li, Y. D. Lin, and S. W. Kuo, *Macromolecules* 44, 9295 (**2011**).
23. J. G. Li, C. Y. Chung, and S. W. Kuo, *J. Mater. Chem.* 22, 18583 (**2012**).
24. C. C. Liu, W. C. Chu, J. G. Li, and S. W. Kuo, *Macromolecules* 47, 6389 (**2014**).
25. N. Suzuki, S. Kiba, and Y. Yamauchi, *J. Nanosci. Nanotechnol.* 12, 983 (**2012**).
26. W. C. Chu, S. F. Chiang, J. G. Li, and S. W. Kuo, *RSC Adv.* 4, 784 (**2014**).
27. J. G. Li, W. C. Chu, U. Jeng, and S. W. Kuo, *Macromol. Chem. Phys.* 214, 2115 (**2013**).
28. W. C. Chu, J. G. Li, C. F. Wang, K. U. Jeong, and S. W. Kuo, *J. Polym. Res.* 20, 1 (**2013**).
29. W. C. Chu, S. F. Chiang, J. G. Li, and S. W. Kuo, *Materials* 6, 5077 (**2013**).
30. D. Hu, Z. Xu, K. Zeng, and S. Zheng, *Macromolecules* 43, 2960 (**2010**).
31. A. R. Balkenende, F. K. D. Theije, and J. C. K. Kriege, *Adv. Mater.* 15, 139 (**2003**).
32. B. Singh, D. D. Gandhi, A. P. Singh, R. Moore, and G. Ramanath, *Appl. Phys. Lett.* 92, 113516 (**2008**).
33. N. Nishiyama, S. Tanaka, Y. Egashira, Y. Oku, and K. Ueyama, *Chem. Mater.* 14, 4229 (**2002**).
34. F. K. de Theije, A. R. Balkenende, M. A. Verheijen, M. R. Baklanov, K. P. Mogilnikov, and Y. Furukawa, *J. Phys. Chem. B* 107, 4280 (**2003**).
35. S. Baskaran, J. Liu, K. Domansky, N. Kohler, X. Li, C. Coyle, G. E. Fryxell, S. Thevuthasan, and R. E. Williford, *Adv. Mater.* 12, 291 (**2000**).
36. C. K. Min, T. B. Wu, W. T. Yang, and C. L. Chen, *Compos. Sci. Technol.* 68, 1570 (**2008**).
37. T. Lee, S. S. Park, Y. Jung, S. Han, D. Han, I. Kim, and C.-S. Ha, *Eur. Polym. J.* 45, 19 (**2009**).
38. J. Lin and X. Wang, *Polymer* 48, 318 (**2007**).
39. N. Suzuki and Y. Yamauchi, *J. Nanosci. Nanotechnol.* 10, 5759 (**2010**).
40. Y. Li, S. Liu, K. Sheng, T. Wei, and X. Wang, *Sci. Adv. Mater.* 7, 2278 (**2015**).
41. Z. Li, L. Wang, X. Ge, H. Ge, and L. Yin, *Sci. Adv. Mater.* 6, 2089 (**2014**).
42. G. Zhu, W. Wang, H. Wang, L. Shan, L. Peng, Q. Zhang, P. Guo, N. Zhou, and L. Zhang, *Nanosci. Nanotechnol. Lett.* 7, 476 (**2015**).
43. G. Chen, Z. Teng, X. Su, Y. Liu, and G. Lu, *J. Biomed. Nanotechnol.* 11, 722 (**2015**).
44. G. Lawrence, C. Anand, E. Strounina, and A. Vinu, *Sci. Adv. Mater.* 6, 1481 (**2014**).
45. H. L. Chen, S. C. Hsiao, T. L. Lin, K. Yamauchi, H. Hasegawa, and T. Hashimoto, *Macromolecules* 34, 671 (**2001**).
46. H. L. Chen, S. Y. Lin, Y. Y. Huang, F. C. Chiu, W. Liou, and J. S. Lin, *Macromolecules* 35, 9434 (**2002**).
47. H. L. Chen, J. C. Wu, T. L. Lin, and J. S. Lin, *Macromolecules* 34, 6936 (**2001**).
48. J. Y. Hsu, I. F. Hsieh, B. Nandan, F. C. Chiu, J. H. Chen, U. S. Jeng, and H. L. Chen, *Macromolecules* 40, 5014 (**2007**).
49. K. W. Huang, L. W. Tsai, and S. W. Kuo, *Polymer* 50, 4876 (**2009**).
50. Y. L. Loo, R. A. Register, A. J. Ryan, and G. T. Dee, *Macromolecules* 34, 8968 (**2001**).

Received: 7 November 2015. Accepted: 4 December 2015.